Verification Testing of a Multi-GNSS RF Signal Simulator

YANHONG KOU AND HAITAO ZHANG
SCHOOL OF ELECTRONIC AND INFORMATION ENGINEERING, BEIHANG UNIVERSITY

GNSS signal and constellation simulators are crucial tools for designing and testing the performance of GNSS user equipment. But how can we be sure of data generated by the simulators? That is, how does one test the test equipment itself? This article describes the features of a multi-GNSS RF signal simulator developed at Beihang University in Beijing, China, and explains how researchers there verified its performance.

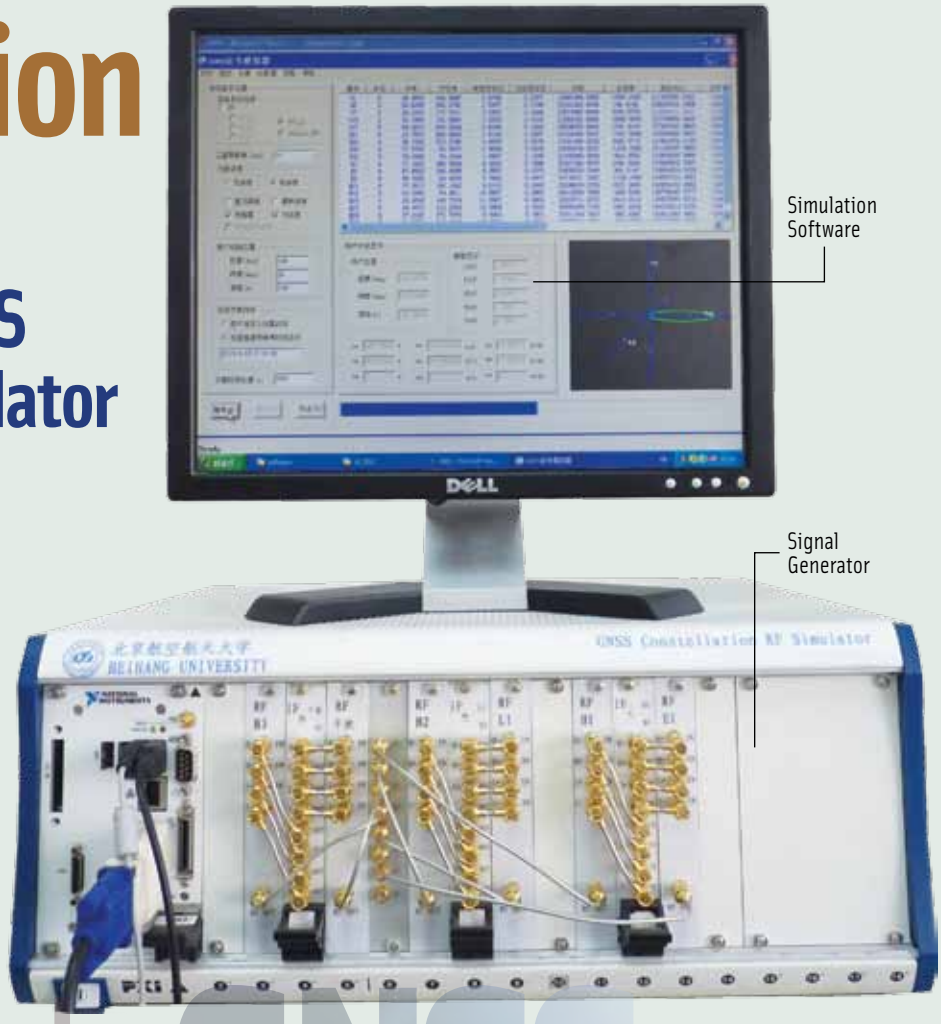

FIGURE 1 Multi-GNSS signal simulator based on PXIe bus

A GNSS signal simulator is mainly used to simulate GNSS signals transmitted by navigation satellites, propagated through the Earth's atmosphere, and received by the receiver antenna. A simulator provides a convenient signal source for the test and validation of receiver function and performance and can also be used in GNSS experiments and studies of signal/data processing algorithms.

A simulator supports controllable and repeatable tests without considering the availability of real satellite signals. Finally, it also allows tests with non-on-orbit satellites, high dynamic, indoor or other critical/specific conditions. Examples of commercial GNSS simulator specifications and articles describing typical applications can be found in the Additional Resource section near the end of this article.

As a key type of test equipment, the GNSS simulator itself needs to be tested extensively to verify that it meets rigorous technical specifications. Although the design of a high-fidelity GNSS RF (radio frequency) signal simulator with capabilities for multi-constellation, multi-signal-structure, multi-channel, and multi-level–output simulation is very challenging, the verification testing of such a simulator could be much more difficult than conducting similar tests for a GNSS receiver. A GNSS simulator has higher requirements for accuracy, precision, stability, range and resolution, not to mention the lack of well-established receivers of new constellations and new signals that could be used in verification testing. This is one of the reasons that few publications are found to explore the issue of simulator testing. The articles by A. Tetewsky *et alia*, P. Boulton *et alia*, and G. Heinrichs *et alia* listed in Additional Resources provide a few examples of such testing.

In order to support the design and validation of new GNSS constellations and signals as well as the corresponding monitoring equipment and receiver

components, our group in Beihang University has developed a fully functioning GNSS constellation simulator capable of real-time simulation of more than 10 kinds of Compass/GPS/Galileo RF signals. One issue raised here is how to prove its qualification for the performance parameters.

After a brief description of its technical characteristics, this article focuses on the verification testing methodology of GNSS RF signal simulators using signals from a variety of constellations. Extensive tests are carried out at the following four levels: analog IF (intermediate frequency)/RF signals, baseband signals, measurements and demodulated navigation messages, and position solutions.

Multi-level measurements of the signal quality are obtained by using a signal quality assessment system incorporating standard instruments, multi-GNSS software receivers, and specialized analysis software with unique signal/data processing techniques to improve observability and measurement accuracy.

Technical Characteristics of the Multi-GNSS Signal Simulator

Two main elements comprise the Beihang University multi-GNSS RF signal simulator: the upper-computer simulation software and the hardware signal generator. The signal generator performs real-time analog IF/RF signal synthesis and includes a synchronization control card, IF signal modulation cards, RF up-conversion and conditioning cards, and RF combining cards. All these cards are mounted as peripheral modules in a PXIe (PXI Express) bus chassis, as described in the patent by Y. Kou *et alia* (2009) cited in Additional Resources.

The upper-computer simulation software performs modeling, signal parameter computation, simulation control, and GUI (graphical user interface). Depending on the computation load, the software can run on the platform of either an embedded PXIe controller mounted on the No. 0 slot of the chassis or a cable-connected PC. The new PXIe specification integrates PCIe (PCI Express) signaling into the PXI standard aiming at instrumentation systems, which provides increased bandwidth, extra timing and synchronization mechanism while ensuring backward compatibility.

The modular architecture based on software radio enables the user to define the combination of constellations, carriers, signals, and interferences to be simulated at will. In addition, the signal generator applies low-IF digital quadrature modulation that can accommodate signals with different structures. So, this design makes it very convenient to increase or decrease the number of simulated constellations and signals, as well as change the signal modulation to support the future signal structures while maintaining the accuracy, resolution, stability, and dynamic range.

Figure 1 shows one configuration of our simulator, which can generate signals on six carrier frequencies simultaneously. The chassis can accommodate up to 10 carriers, with each three-card module generating signals on two carriers in our design. The signal generator can be conveniently integrated with other modular measurement instruments while a specially designed synchronization control card and RF signal-combining card support seamless extension of the multi-chassis.

Other characteristics of the simulator include:

1. Multi-level output: providing baseband data, analog IF signal, and RF signal output simultaneously to facilitate multi-loop test and receiver troubleshooting
2. Multi-constellation navigation data and multi-structure signal simulation: supporting multi-frequency/multi-system/multi-mode integration navigation experiments and receiver tests
3. Two-level power control: wide range power control of the RF/IF signals for all the simulated space vehicles (SVs)
4. High dynamic, variable interference, and multipath simulation: various user dynamics simulation using a common trajectory generation method, CW (continuous wave) /narrow-band /wide-band /swept-frequency interferences generation with controllable parameters on different center frequencies, multipath modeling and error envelop testing
5. Real-time simulation: real-time signal calculation and generation of unlimited time length
6. Observability: various intermediate outputs for test and analysis of physical signals, measurements, and navigation solutions
7. Controllability: definable and repeatable simulation scenarios, optional signal formats, configurable parameters including error models, combination of signals and interferences, signal/interference parameters, trajectory dynamics, SV shielding angle, constellation, ephemeris source, and so forth.

Four-Level Verification Testing

For an effective test of the corresponding receiver performance, signals generated by a simulator should have much higher accuracy, precision, stability, resolution, and wider range, as can be checked in the simulator's technical specifications. Generally, the simulated signals are spreading signals buried in the thermal noise, which are difficult to be characterized using regular measurement techniques.

The verification testing of a multi-constellation, multi-signal-structure, multi-channel, multi-level simulator could be much more difficult than conducting similar tests for a GNSS receiver.

Ideally, we would like to choose the analog IF/RF output of the simulator as the test port and try to obtain black-box testing results of the functions and performances of the simulator, using a signal-quality assessment system including standard instruments, multi-GNSS software receivers and specialized analysis software.

Simulator output signals	Instruments	Performance Metrics
High SNR (constant SNR higher than 20dB) CW signal or interference	High accuracy frequency counter	Carrier frequency accuracy, resolution, and stability
	High accuracy power meter	Control range, accuracy, resolution, and stability of the power level
	Digital spectrum analyzer / phase noise analyzer	Phase noise, spur, and harmonics, frequency transfer function of the signal channel (Enough frequency points within the bandwidth should be tested)
High SNR (constant SNR higher than 20dB), zero-Doppler, single-channel modulated signal	Real-time spectrum analyzer	Frequency domain characteristics: power spectrum, bandwidth, etc.
	High speed oscilloscope	Time domain characteristics: waveforms, eye-diagrams, chip transitions, etc.
	Vector signal analyzer	Modulation domain characteristics: vector/constellation/scatter plot, error vector magnitude (EVM), I/Q quadrature and balance, amplitude/phase/frequency errors, etc.

TABLE 1. Testing the analog IF/RF signals using standard instruments

The method lowers the requirements on the testability design of the simulator and turns our attention from internal implementation of the simulator to the RF/IF output and several necessary test-case signals, such as unmodulated CW signals. By using this approach, we do not need to open the simulator chassis to access its internal test points or to embed extra test programming into the simulator software. This may make things more difficult than "white-box" testing to obtain particular results, but the test applicability and operability are enhanced.

We test the RF/IF output signals at four levels — analog IF/RF signals, baseband signals, measurements and navigation data, and navigation solutions. In the following sections we describe our verification test procedures and the results in these areas using the Beihang University GNSS simulator.

Analog IF/RF Signals

The analog IF/RF output signals of the simulator can be sent to various standard instruments. **Table 1** summarizes the main test items, necessary instruments, and performance metrics. To minimize the measurement error caused by thermal noise, the instrument input SNR (signal to noise ratio) is typically required to be higher than 20 decibels.

The analog IF output of our simulator reaches up to -43dBW, which can be tested directly. Most simulators provide a calibration/monitoring port for high-power–level RF signal output. For example, the power level of the calibration port of our simulator is 40 decibels higher than the nominal RF signals.

As an example, **Figure 2(a)** shows the power spectrum of the combined five RF signals (GPS L1 C/A, Galileo GIOVE-A E1B, Compass B1I, B2I, B3I). The controlled signal power is –110dBW + 40dB = –70dBW = –40dBm. **Figure 2(b)** shows the power spectrum of the GPS L1C IF signal. The high power level at the IF output yields a clearer view compared to the RF signal.

Figure 3 shows the power spectrum of the swept frequency interference with a bandwidth of 20 megahertz, a period of 0.5 milliseconds, and a center frequency of 1.4 gigahertz. The spectrum plot also reflects the amplitude-frequency response of the RF channel within the 1.39~1.41gigahertz band.

Figure 4 shows the constellation plot, the error vector magnitude (EVM), the power spectrum, and the statistical values of modulation quality parameters measured by the vector signal analyzer for the Compass B1 QPSK-R(2) IF signals generated by the simulator. **Figure 5** is the eye-diagram of the baseband signals demodulated by the analyzer.

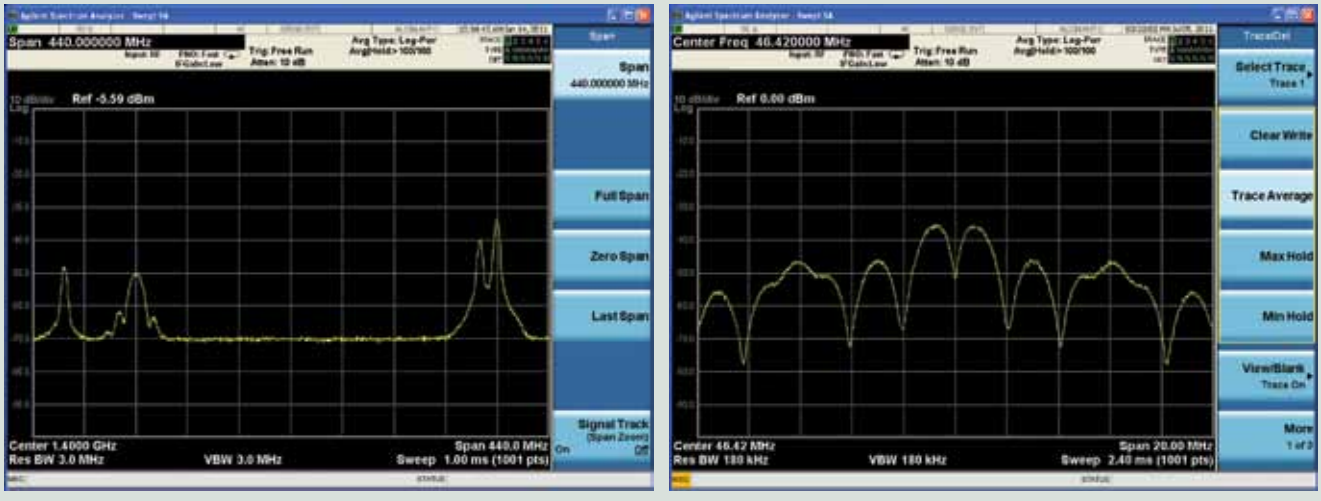

(a) RF signals (b) GPS L1C analog IF signal

FIGURE 2 Power spectrum density (PSD) plot

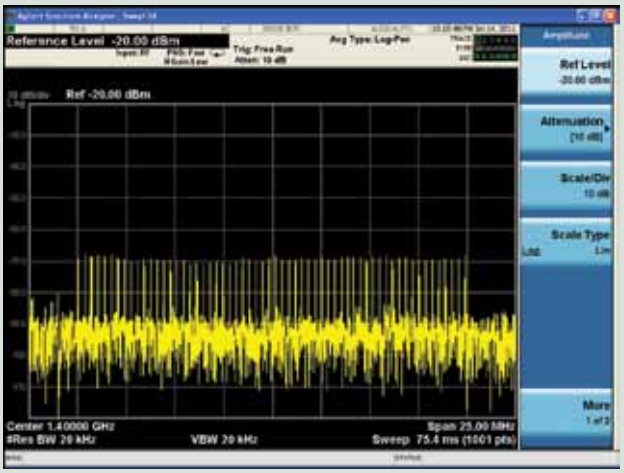

FIGURE 3 PSD of swept frequency interference signal

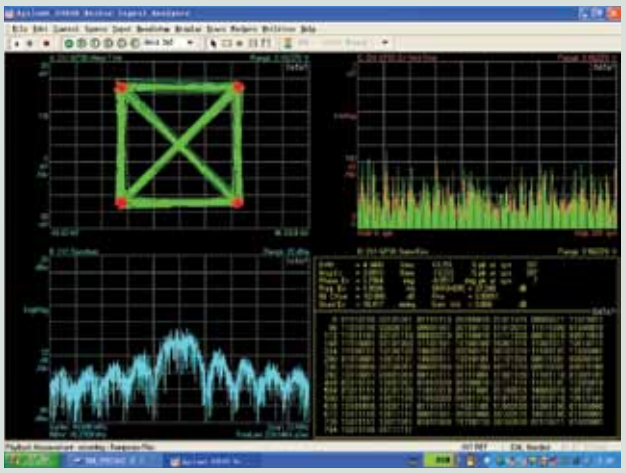

FIGURE 4 Modulation domain test using a vector signal analyzer

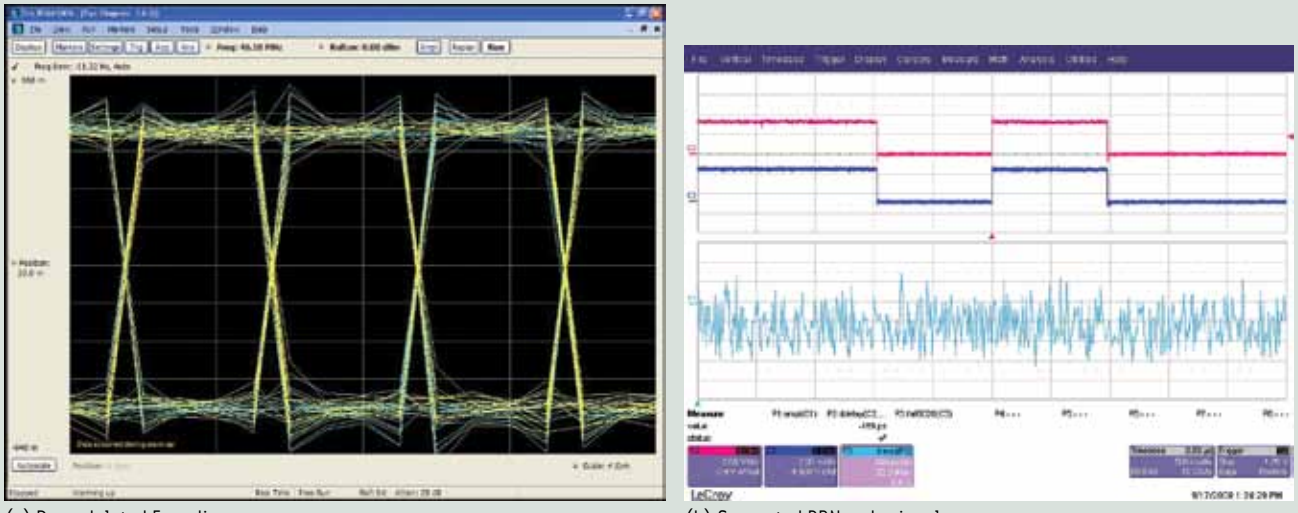

(a) Demodulated Eye-diagram

(b) Generated PRN code signals

FIGURE 5 Demodulated/generated baseband signal waveforms

In contrast, the simulator designer can draw two digital channel outputs simulating the same baseband PRN (pseudorandom noise) code waveforms to the high-speed oscilloscope to measure the time alignment error of chip transitions, as illustrated in **Figure 5(b)**. This is a direct measurement of the inter-channel coherence and bias without a demodulation process. However, it is neither applicable to the third-party tester nor to the user.

Baseband Signals

The standard instrumentation is only capable of measuring communication system–related parameters of the IF/RF signals specialized for the test case. It cannot measure parameters showing the distortion effects on navigation performance. Nor can it measure the signals with nominal RF power level or under dynamic scenarios.

To solve this problem, we propose a customized GNSS signal-quality assessment system based on high-speed data acquisition equipment, a multi-GNSS software receiver, and a baseband signal analysis software, as illustrated in **Figure 6**. The raw IF/RF signals are collected by the high-speed data acquisition equipment and sent to the software receiver. After signal acquisition and tracking, we calibrate the sampling frequency online as described in the article by Y. Kou *et alia* (2010), wipe off the carrier (including the Doppler) and the data to get the baseband PRN code signal, periodically average the signal to maximize SNR, then analyze its characteristics in the amplitude, time, frequency, modulation, and correlation domains. Further assessment can be done based on the extracted measurements, demodulated navigation data, and PVT (position, velocity, time) solution from the software receiver.

This system not only realizes a set of software/virtual instruments to take the place of the aforementioned standard instrumentation including the oscilloscope, the spectrum analyzer, and the vector signal analyzer. It also goes deep into the correlation domain, the measurement domain, the navigation data domain, and the navigation solution domain to assess the parameters tied up with navigation performance.

Some unique signal-processing techniques are applied to increase the C/N_0 (carrier to noise ratio), remove the carrier (including the carrier Doppler), and calibrate the sampling frequency to improve the signal observability and assessment accuracy, while reducing the requirements for the testability design of the simulator.

Our system can measure the nominal output signals from the simulator rather than requiring a high-power–level, single-channel, unmodulated CW signal or a modulated signal with zero Doppler. When the specialized test case signal is available, it can achieve more accurate, comprehensive, and realistic test results compared to the conventional instruments.

In our proof-test we use the direct RF sampling front-end developed by our group (described in the article by H. Liu *et alia*) to collect the raw RF signals. The front-end embodies only amplifiers and filters in its RF chain. The RF/IF signals are sampled by an analog/digital converter (ADC), transmitted by a gigabit Ethernet to a computer for storage and processing. The wideband filter in the signal path mitigates the effects of the instrument-induced signal distortion and correlation loss on the test results.

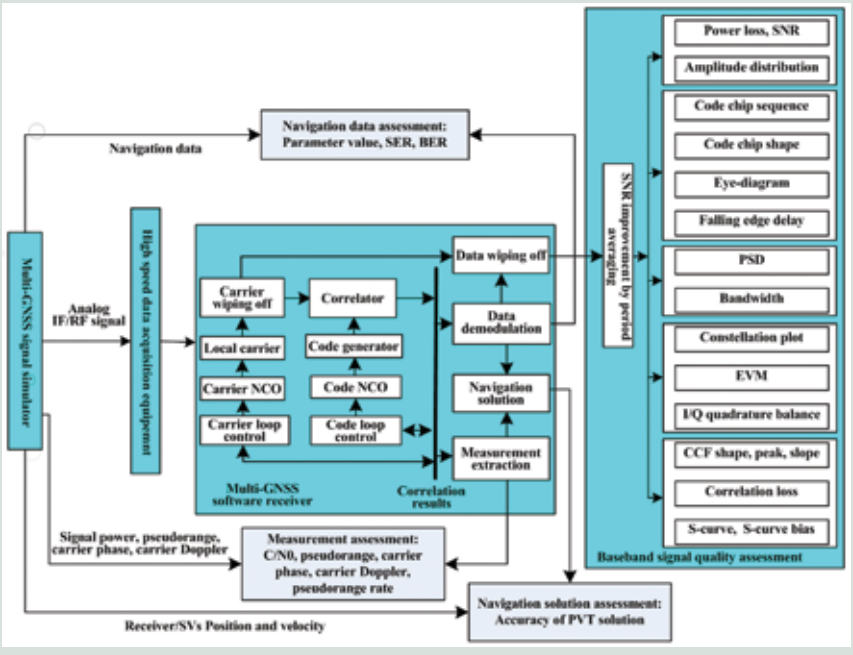

FIGURE 6 GNSS signal quality assessment system

As described in the article by M. Pini *et alia*, the signal (in-phase component) to be analyzed with its carrier and data wiped off by the software receiver is a period signal with the same period as the PRN code:

$$I[i] = Ac_F(iT_s) + n_c(iT_s) \quad (1)$$

where $c_F(iT_s)$ is the ith sample of the filtered baseband PRN code signal in one code period and $n_C(iT_s)$ is the ith sample of the band-limited in-phase noise component. The signal after R periods' averaging is

$$I_A[i] = \frac{1}{R}\sum_{J=1}^{R} I^J[i] = \frac{1}{R}\sum_{J=1}^{R}[Ac_F^J(iT_s) + n_c^J(iT_s)] \quad (2)$$

where the superscript J represents the Jth period.

Rewrite (2) as follows:

$$I_A[i] = \underbrace{A\cdot\left[\frac{1}{R}\sum_{J=1}^{R} c_F^J(iT_s)\right]}_{C_A[i]} + \underbrace{\left[\frac{1}{R}\sum_{J=1}^{R} n_c^J(iT_s)\right]}_{N_A[i]} = C_A[i] + N_A[i] \quad (3)$$

where $C_A[i]$ is the ith sample of the PRN code signal after R periods averaging. The signal power remains the same as before averaging. $N_A[i]$ is the ith sample of the noise.

Because the ith noise samples in each period are statistically independent, the noise power after averaging reduced to $1/R$ of the original value. Thus, the SNR is improved by R times. (One precondition is that the sampling frequency is accurate enough, which can be achieved by the calibration process proposed in the article by Y. Kou *et alia* [2010]). The digital samples with improved SNR can be directly characterized by the subsequent software.

The following analysis uses the GPS L1 C/A signals collected from the nominal-power RF output port of the simulator picking out the RF signal from PRN17, which has a power level of –140 dBW at a satellite elevation of 78 degrees.

The **Figure 7** series provides various measurements of the signal quality of the baseband signals. The baseband signal waveform in **Figure 7(a)** and the amplitude distribution histogram in **Figure 7(b)** demonstrate the effect of the periodic averaging: the raw signal is buried in noise, with its waveform/amplitude being indistinguishable and its quality unavailable. After 100-period averaging, the SNR is improved by about 20

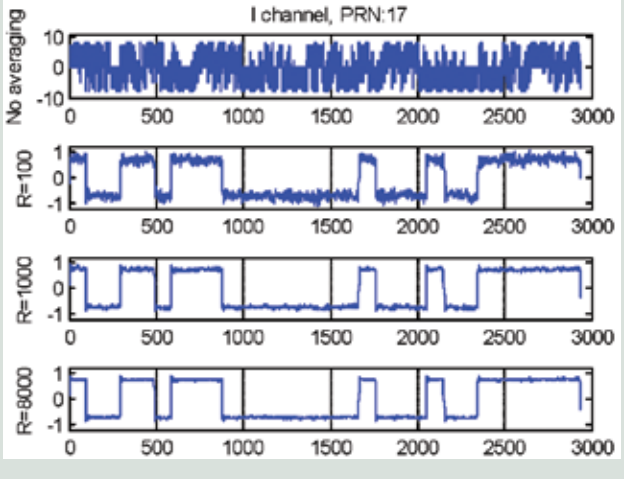

FIGURE 7a SNR improvement via periodic averaging: time domain waveform

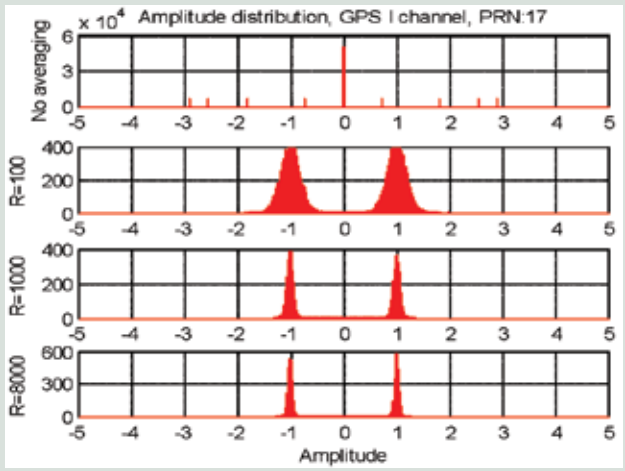

FIGURE 7b SNR improvement via periodic averaging: amplitude distribution histogram

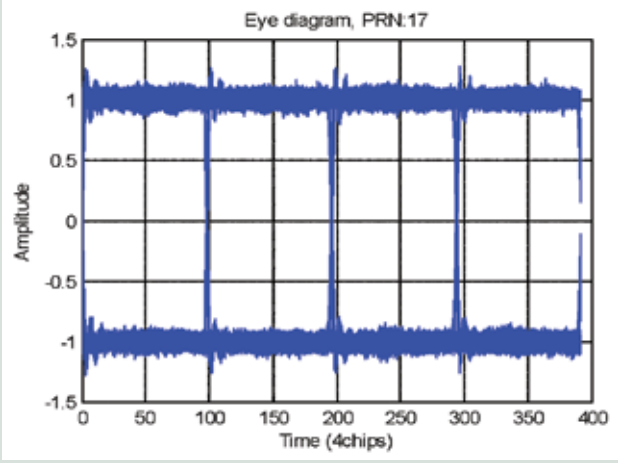

FIGURE 7c Eye diagram

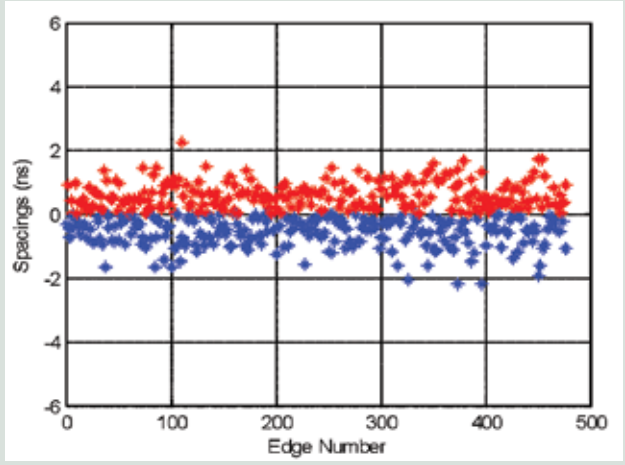

FIGURE 7d Measurements of the code chip zero-crossing point

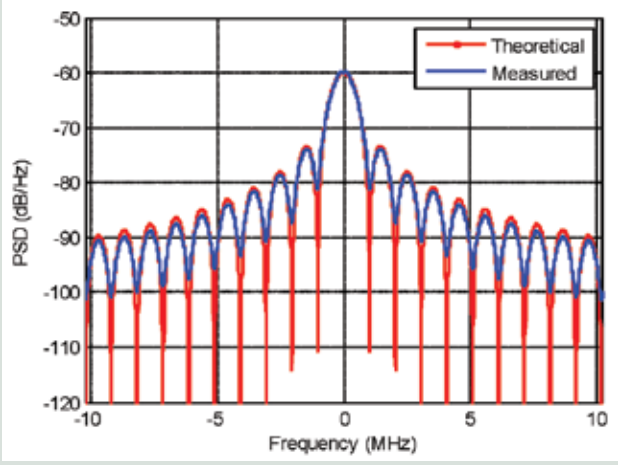

FIGURE 7e Measured PSD using Welch's modified periodogram method

decibels. So, the code chips can be discerned easily, and two Gaussian distributions around the normalized PRN code amplitude (+1/-1) are present.

When the averaging window extends to 8,000 periods, the SNR is increased by 39 decibels, and the code chip shape becomes very clear with the noise suppressed sufficiently. The two Gaussian distributions become narrow and concentrated on their mean values with very small variance. Now we can analyze the averaged signal directly.

The trace of the eye-diagram in **Figure 7(c)** is quite clear and rectangular. The steep transition reflects the wideband filter characteristics of the RF chain of the simulator and indicates an accurate sampling frequency in the processing. It also promises a small analog distortion (TMB distortion), a sharp auto-correlation peak, and a low correlation loss. The unidentifiable zero-crossing point bias promises a very small digital distortion (TMA distortion). **Figure 7(d)** calculates the zero-crossing point's delay. The mean value of the falling edge's delay of the code chips is 0.64 nanoseconds.

Figure 7(e) shows the measured power spectrum density (PSD) of the baseband signal using Welch's modified periodogram method (the blue line), which fits into the theoretical spectrum (the red line) of BPSK-R(1) signal very well. The similarity coefficient of the two spectrum between –10MHz ~ +10MHz reaches 0.999097.

Figure 7(f) measured the CCF (cross correlation function, the black line) between the baseband signal and the local PRN17 code, which fits into the ACF (auto-correlation function, the red line) of the local PRN17 code very well. The normalized CCF peak value is 0.9967, corresponding to a correlation loss of 0.0284 decibel.

Figure 7(g) and **7(h)** show, respectively, the S-curves and S-curve biases with various correlator spacings. The maximum pseudorange bias caused by the signal distortion (the relative lock-point bias) is 2,670.5 picoseconds, which is located at a correlator spacing of 0.1chips.

As an example of the signal analyzer function of the software receiver, **Figure 8** shows the regular fast Fourier transform (FFT) circular correlation results using the GPS L1C software receiver to acquire the analog IF L1C signal gener-

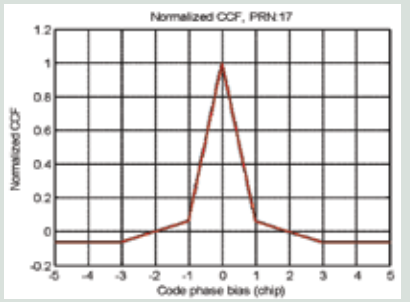

FIGURE 7f Normalized cross correlation function

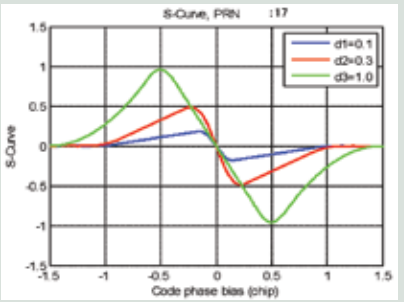

FIGURE 7g S-curves with various correlator spacings

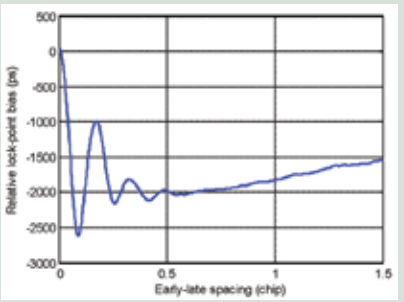

FIGURE 7h Relative lock-point bias (S-curves bias)

ated by the simulator. Typical CCF peak and side-lobes of TMBOC(6,1,4/33) signals are very clear.

Figure 9 uses CCF analysis to detect the multipath signals added to Compass PRN2 and PRN3 B1 signals by the simulator. The multipath delay (120 nanoseconds) and the amplitude attenuation coefficients (0.5 and 0.8, respectively) can be roughly estimated using a polyline fitting method.

Measurements and Navigation Data

Our simulator can record the power level, propagation delay, each ranging error, navigation data, or other parameters of the simulated GNSS signals. A receiver capable of processing the corresponding signals can estimate the C/N_0, pseudorange, carrier Doppler, and carrier phase of each SV signal, or record the demodulated navigation data. Thus, we can verify the correctness of the signal/data simulation.

Using specific test scenario configurations and specific data processing, we can even evaluate the accuracy and range of some parameters of the signals generated by the simulator. To eliminate the effects of extra clock error, clock drift, and frequency drift, the receiver or the signal collecting equipment should use a clock reference coherently derived from the simulator clock reference.

Figure 10 shows the C/N_0s of five GPS SV signals estimated by a commercial receiver, which validates the relative power control between different SVs in the simulator.

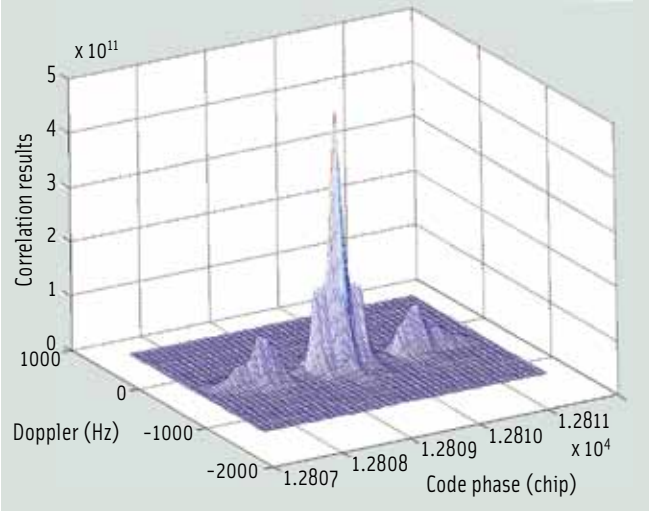

FIGURE 8 FFT acquisition results of generated L1C signals

For the simulator, we can measure the accuracy of pseudorange, carrier phase, and carrier Doppler of the simulated signals using several approaches. One approach with the simplest data postprocessing requires a test scenario of a static SV and a static receiver platform, or using two channels to generate the same SV signals. The receiver processes the signals and performs a zero-baseline analysis. This requires special test-case signal generation in the simulator instead of recording the simulated signal parameters.

Figure 11 shows the pseudorange error and carrier phase error of the GPS L1C signal generated by the simulator, collected by the direct RF sampling front-end and measured by the software receiver. The standard deviations are 0.06939 meters and 0.00033 meters, respectively.

Note that such errors are actually contributed by both the simulator — a simulation error (mainly caused by the modeling errors and digital/analog signal distortions) — and the receiver measurement error (mainly caused by thermal noise and clock jitter). Differentiating between these types of errors by traditional data processing is difficult.

The effect of thermal noise and clock jitter can be simply reduced by long-term averaging. However, the simulator control error will also be blurred during this processing. Nevertheless, we can still try to reduce the contribution of receiver measurement error in order to estimate the simulator error in several ways: improving the SNR, using a highly stable coherent clock, tuning the loop parameters, maximizing pre-correlation integration time, using proper filtering, and so forth.

The simulator control resolution and relative bias can be accurately measured using long-term averaging. **Figure 12** shows the receiver data processing results for the simulator code-rate control resolution test using –160dBW GPS L1 C/A signals. The blue line is the receiver-measured pseudorange difference of two simulator configurations with a code-rate difference of one control step, whereas the red line is the fitted line with its slope (0.003 m/s) representing the control step/resolution of the simulator code-rate.

Navigation Solutions

The navigation solutions enable a general assessment of the overall performance of the simulator. **Figure 13** shows the positioning error of GPS L1C signals generated by the simula-

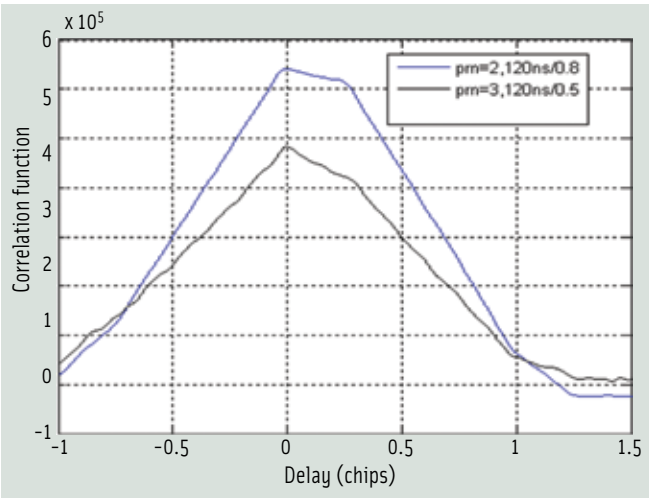

FIGURE 9 Measured CCF and multipath parameters of simulator-generated Compass PRN2 and PRN3 B1I signals

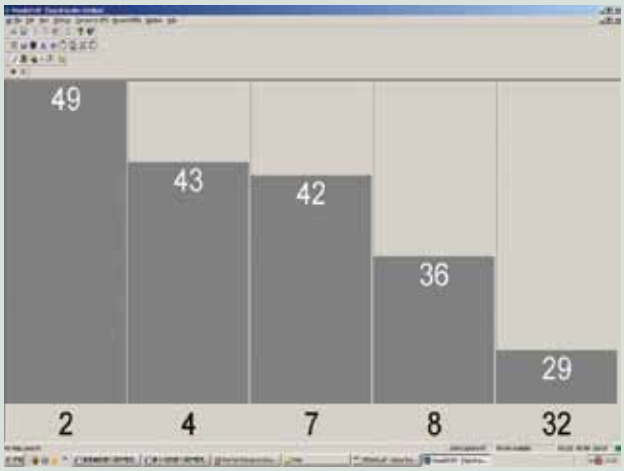

FIGURE 10 C/N_0 monitoring of GPS satellites in view using a commercial receiver

tor and processed by the software receiver. The results validate the correctness of the simulated navigation data (in GPS NAV format for the time being) and L1C signals.

For the error analysis of the closed-loop test under normal dynamic scenarios, one problem is how to align the time of the receiver-solved PVTs with the simulator-generated data. Our approach, based on a receiver design that enables true PVT solution, reports the measurements/navigation solutions on integer seconds of system time.

The accuracy of the receiver reporting time epochs reaches tens of nanoseconds (or even better) after clock error correction, whereas the simulator just records its signal parameters and trajectory according to the simulated time of reception aligned with integer seconds of system time. Thus, the extra error caused by the time misalignment during data comparison can be disregarded.

Figure 14 shows the dual-system positioning results using a commercial Compass/GPS receiver. The navigation solutions include the simulated B1I signals of seven Compass SVs in view and L1 C/A signals of eight GPS SVs in view. The signal strength of each SV channel, and the positioning precision are also shown.

Conclusions

The four-level verification testing methodology is not limited by the internal implementation of various simulators. It enables a direct test of RF/IF output, which reduced the testability design requirements of simulators, and thus is more applicable and operable than white-box testing. The method provides an accurate multi-level description of the signal quality.

The signal quality assessment system that we have developed can measure not only typical communication system–related parameters but also signal distortions affecting navigation performance. By applying special signal/data processing techniques to improve signal observability and measurement accuracy, we can characterize not only the high-power–level

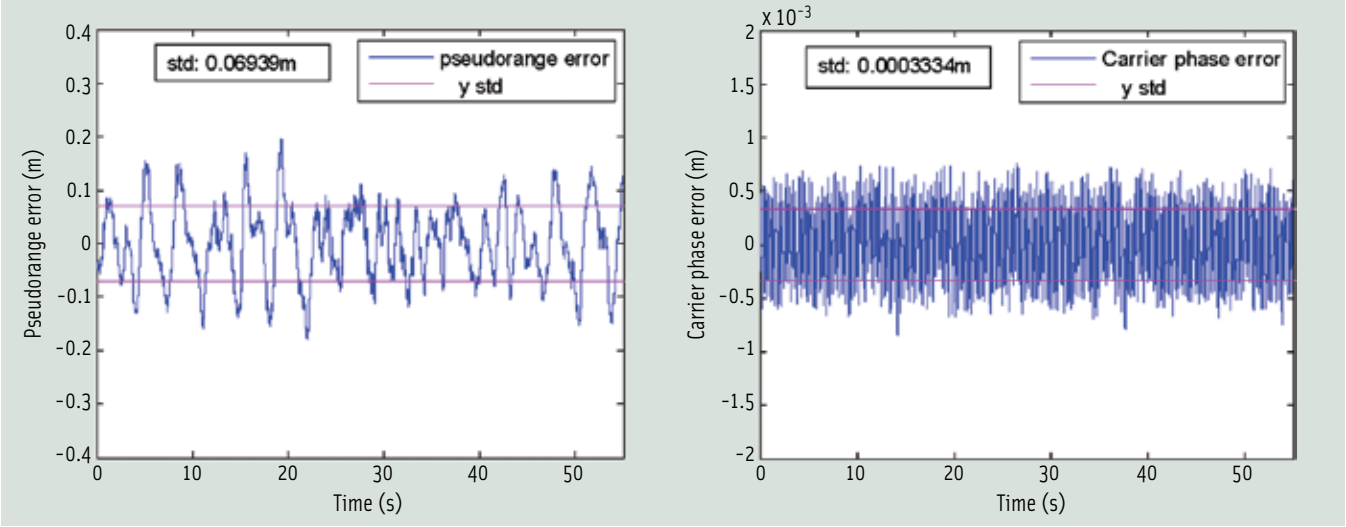

FIGURE 11 Receiver-measured pseudorange error and carrier phase error of GPS L1C signal

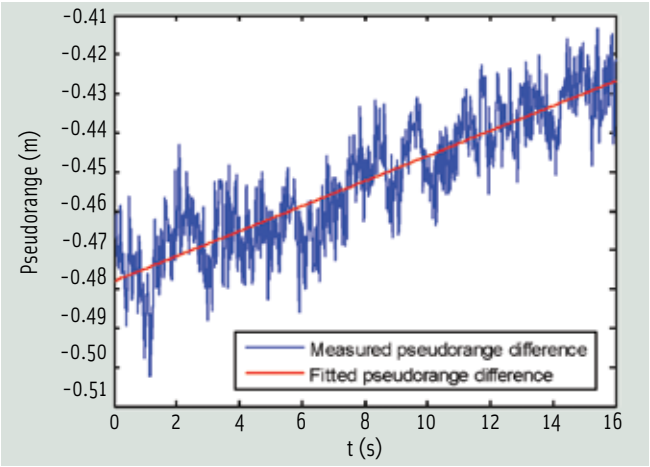

FIGURE 12 Receiver-measured control step of code rate of the simulator

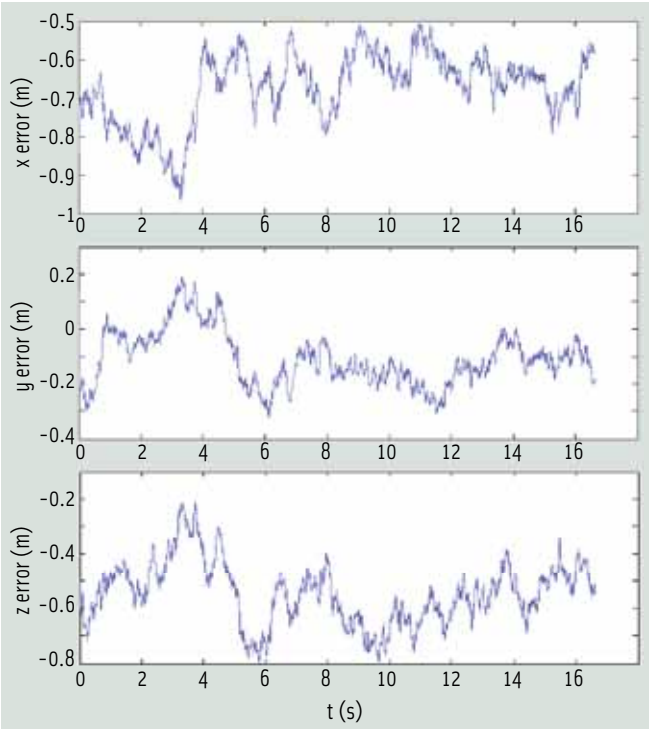

FIGURE 13 Closed-loop positioning error of GPS L1C signal simulator and software receiver

zero-Doppler test signals but also the normal dynamic signals buried in thermal noise.

A possible extension of this work is to further explore methods for testing various aspects of the technical performance of GNSS signal simulators, including both essential mathematical analysis and extensive experimental validation.

Acknowledgement

This article is based on a paper presented at the 2nd China Satellite Navigation Conference (CSNC 2011) held May 18–20, 2011, in Shanghai, China.

Manufacturers

The BUAA-EE-SIM GS200 multi-GNSS RF signal simulator, the Multi-GNSS software receiver, and the direct RF signal sampling frontend are developed by the **School of Electronic and Information Engineering, Beihang University,** Beijing, China. The chassis is the NI PXIe-1075 from **National Instruments Corporation**, Austin, Texas, USA. The analog IF/RF signal test uses an Agilent N9010A spectrum analyzer and an Agilent 89601A vector signal analyzer from **Agilent Technologies, Inc.**, Santa Clara, California, USA, a Tektronix RSA6100A real-time spectrum analyzer from **Tektronix, Inc.**, Beaverton, Oregon, USA, and a LeCroy WavePro 7300 digital oscilloscope from **LeCroy Corporation**, New York, New York, USA. Our dual-system positioning test used the commercial Compass/GPS receiver UR240-CORS from **Unicorecomm Co., Ltd.**, Beijing, China.

Additional Resources

[1] Artaud, G., and A. de Latour, J. Dantepal, L. Ries, Maury, N., Denis, J.-C., Senant, E., Bany, T., "A New GNSS Multi Constellation Simulator: NAVYS," *Proceedings of the 23rd International Technical Meeting of The Satellite Division of the Institute of Navigation (ION GNSS 2010)*, Portland, OR, September 2010, pp. 845–857

[2] Berglez, P., and E. Wasle, J. Seybold, and B. Hofmann-Wellenhof, "GNSS Constellation and Performance Simulator for Testing and Certification," *Proceedings of the 22nd International Technical Meeting of The Satellite Division of the Institute of Navigation (ION GNSS 2009)*, Savannah, GA, September 2009, pp. 2220–2228

[3] Boulton, P., and A. Read, and R. Wong, "Formal Verification Testing of Galileo RF Constellation Simulators," *Proceedings of the 20th International Technical Meeting of the Satellite Division of The Institute of Navigation (ION GNSS 2007)*, Fort Worth, Texas, September 2007, pp. 1564–1575

[4] Han, L., and Y. Kou, "Simulation and assessment of GPS signal quality degradation caused by satellite hardware failures", *Proceedings of SCIRP CPGPS 2010*, August 18–20, 2010, Shanghai, China

[5] Heinrichs, G., and M. Irsigler, R. Wolf, and G. Prokoph, "Performance Evaluation of the Multi-Constellation and Multi-Frequency GNSS RF Navigation Constellation Simulator NavX-NCS," *Proceedings of the 21st International Technical Meeting of the Satellite Division of The Institute of Navigation (ION GNSS 2008)*, Savannah, GA, September 2008, pp. 1237–1241

[6] http://www.castnav.com/cast_pdf/cast_2000.pdf

[7] http://www.ifen.com/content/flyer/NavX-NCS-PRO-Datasheet_July2010.pdf

[8] http://www.spirent.com/Solutions-Directory/~/media/Datasheets/Positioning/GSS8000.ashx

[9] Kou, Y., (2008), and B. Zhang, and Y. Zhao, "Design and Implementation of a Multi-Signal-Structure GNSS Signal Simulator Using Low IF Digital Quadrature Modulation", *Proceedings of the 21st International Technical Meeting of the Satellite Division of The Institute of Navigation (ION GNSS 2008)*, Savannah, GA, September 2008, pp. 2677–2691

[10] Kou, Y. (2009), and H. Liu, H. Zhang, B. Yu, and Z. Wang, "Method and Apparatus for Implementation of a GNSS Signal Simulator Based on PXIe Bus," Chinese patent No. 200910238050.2, 2009

[11] Kou, Y. (2010) and X. Zhou, Y. Morton, and D. Akos, "A Software-Based Receiver Sampling Frequency Calibration Technique and its Application in GPS Signal Quality Monitoring," *Proceedings of IEEE/ION PLANS 2010*, Indian Wells, California, USA, May 2010, pp. 718–727

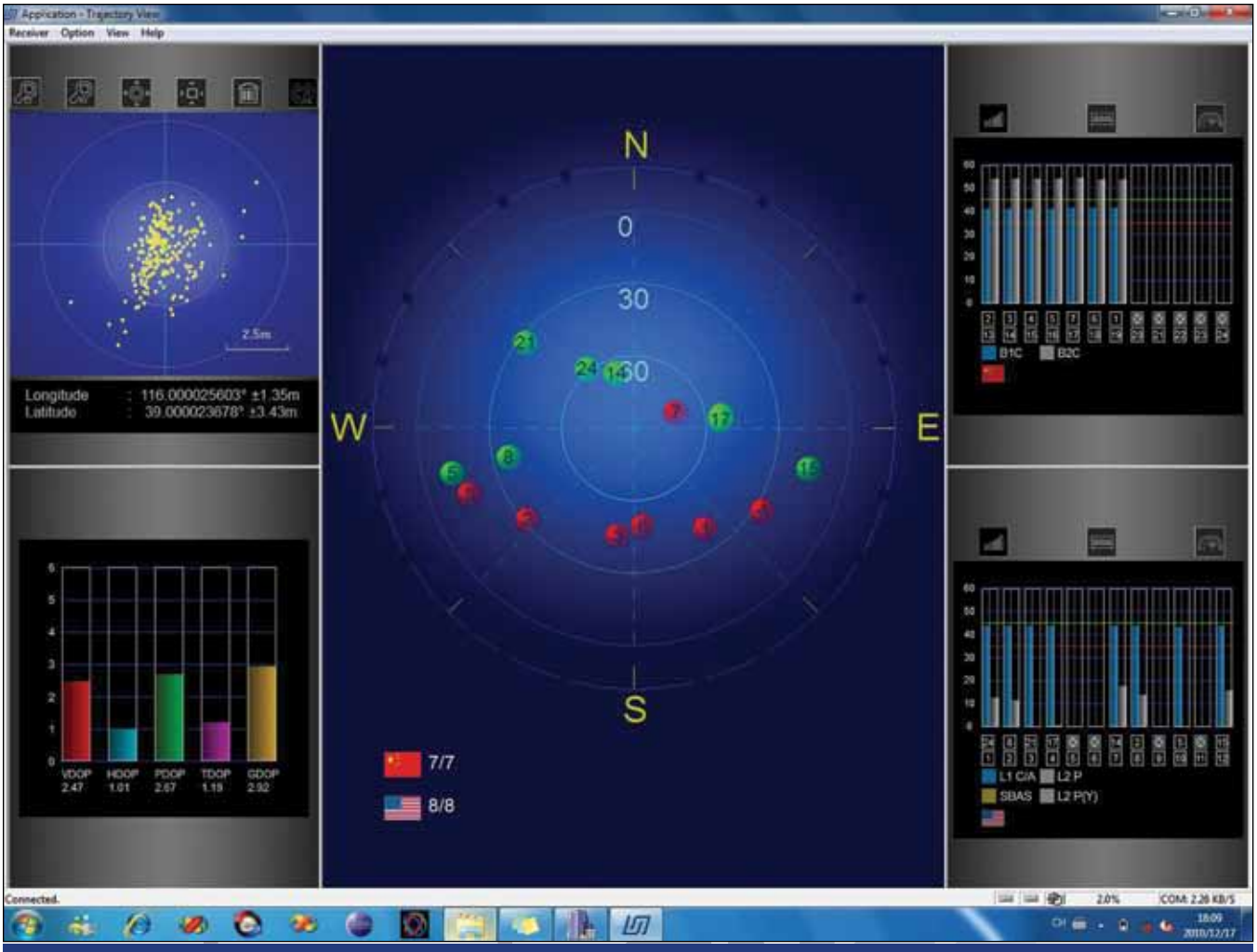

FIGURE 14 Positioning result using a commercial Compass/GPS receiver

[12] Kou, Y., and Z. Ma, B. Zhang, Q. Zhang, and J. Zhang, "Common navigation satellite signal interference and signal generation method", Chinese patent No. 200810117348.3, 2008

[13] Li, R., and D. Zeng, T. Long, and L. Zhang, "Architecture and Implementation of a Universal Real-Time GNSS Signal Simulator," *Proceedings of the 2010 International Technical Meeting of The Institute of Navigation*, San Diego, California, USA, January 2010, pp. 1037–1043

[14] Liu, H., and Y. Kou, "Design and Implementation of a GNSS Signal Collection System Using Direct RF Sampling", *Proceedings of IEEE Prime Asia 2009*, Shanghai, China, Nov. 19–21, 2009

[15] Liu, Q., and Y. Kou and H. Zhou, "Design and Implementation of a Real-time L2C IF Signal Simulator," *Proceedings of IEEE ICISE 2010*

[16] National Instruments Corporation, NI PXIe-1075 User Manual, July 2008

[17] Pini, M., and D. Akos, "Exploiting GNSS Signal Structure to Enhance Observability," *IEEE Transactions on Aerospace and Electronic Systems*, VOL. 43(4), October 2007, pp. 1553–1566

[18] PXI Systems Alliance, PXI-5 PXI Express Hardware Specification, Revision 1.0

[19] Tetewsky, A., and A. Soltz, D. Fuhry, G. Barton, D. Eyring, B. Goossens, M. Dodds, and L. Fava, "Validating the Validating Tool: Defining and Measuring GPS Simulator Specifications," *Proceedings of the 10th International Technical Meeting of the Satellite Division of The Institute of Navigation (ION GPS 1997)*, Kansas City, Missouri, USA, September 1997, pp. 1681-1695

[20] Yang, W., and Y. Zhao, Y. Kou, and Z. Huang, "Modeling of GPS multi-path signals and receiver testing," *Journal of Beijing University of Aeronautics and Astronautics*, 2009,V35(5): pp. 551-554

[21] Zhao, Y., and Y. Kou, Z. Huang, and Q. Zhang, "A Common trajectory generation method of three-dimensional vector for GNSS simulator," Chinese patent No. 201010296636.7, 2010

Authors

Yanhong Kou is an associate professor in School of Electronic and Information Engineering at Beihang University. She received a Ph.D. in Communication and Information Engineering from Beihang University. Since 2002, she has been working on a wide range of GNSS-related research areas. Her research interests include GNSS signal simulators, high performance receivers, and digital signal processing.

Haitao Zhang is a master's degree candidate in School of Electronic and Information Engineering at Beihang University. He received his bachelor degree in Measurement and Control Technology and Instruments from Wuhan University of Technology. His research interests include GNSS signal simulators and hardware design. IG